Available online at www.sciencedirect.com
ScienceDirect
Trans. Nonferrous Met. Soc. China 26(2016) 767−774
Transactions of Nonferrous Metals Society of China
www.tnmsc.cn

Effect of catalytic activities of mixed nano ferrites of zinc and copper on decomposition kinetics of lanthanum oxalate hydrate

H. NAYAK

Department of Chemistry, Orissa University of Agriculture and Technology, Bhubaneswar 751003(Orissa), India

Received 10 April 2015; accepted 31 October 2015

Abstract: Nanostructured zinc−copper mixed ferrite was synthesized using sol−gel method. Different compositions of ferrite, $Zn_{(1-x)}Cu_xFe_2O_4$ (x=0.0, 0.25, 0.50, 0.75), characterized by XRD, reveal single phase inverse spinel in all the samples. With increasing copper content, the crystallite size increases. The surface morphology of all the samples, studied by SEM, shows porous structure of particles. The prepared samples were also analyzed by FT-IR and TEM. Catalytic activity of the samples was studied on lanthanum oxalate decomposition by thermogravimety .The rate constant k has the highest value with x=0.75 and 5% (mole fraction) of the catalyst and is attributed to high copper content, the mixed sites Cu^{2+}−Fe^{+} and/or Cu^{+}−Fe^{2+} ion pairs besides the one component sites Cu^{2+}−Cu^{+}, Fe^{3+}−Fe^{2+}, as a result of mutual charge interaction. In other words, the increasing activity of mixed oxides is attributed to increase in the content of active sites via creation of new ion pairs. With increasing Zn content, particle size increases. Variation of catalytic activity of ferrite powders is due to the changes of the valence state of catalytically active components of the ferrites, which oxidizes the carbon monoxide released from lanthanum oxalate.

Key words: mixed ferrite; spinel; valence induction; catalyst activity; rate constant; lanthanum oxalate

1 Introduction

Ferrite is an important class of material that has potential applications in integrated circuitry, transformer cores and magnetic recording [1,2]. The study of ferrites has attracted immense attention of the scientific community because of their novel properties and technological applications especially when the size of the particles approaches to nanometer scale.

The study of ferrite nanoparticles is of interest due to the fundamental difference in their magnetic and electronic properties compared with the bulk counterparts. Nano oxides due to their electrical properties have been found to be good catalysts, as compared to their corresponding normal oxides [3]. $Ni_{0.5}M_{0.5}Fe_2O_4$ (M=Co, Cu) ferrite nanoparticles synthesized using citrate precursor method, annealed at temperatures of 400, 450, 500 and 550 ℃ [4], display cubic spinel structure up to 450 ℃, and at temperature higher than 450 ℃ display a tetragonal structure, suggesting that nucleation/growth mechanism is different at temperatures above and below a critical temperature in this range. $Ni_{0.5}M_{0.5}Fe_2O_4$ ferrite doped with 0.1 and 0.4 mol Cu behaves as a catalyst [5].

A comparative analysis of the two catalysts indicated that the catalyst doped with 0.4 mol Cu showed better performance. The nickel substituted copper ferrite nanoparticles ($Ni_xCu_{1-x}Fe_2O_4$, x=0, 0.2, 0.4, 0.6, 0.8, 1.0) were found to have better catalytic activity as compared to the corresponding metal oxides [6].

A study on the thermal decomposition of the lanthanum oxalate hydrate and its mixtures in 5% (mole fraction) with transition metal nano oxide compounds (TMNOCs), viz., CuO, Fe_2O_3, TiO_2 and Cr_2O_3 has been carried out and the results reveal that other than CuO, the oxides have a retarding effect on the decomposition rate [7]. The Zn^{2+} substitution in ferrites, i.e., cobalt–zinc ferrite nano-particles $Co_{1-x}Zn_xFe_2O_4$, observed variation in crystalline size and the structural properties of ferrite nano-particles [8]. The $Ni_{1-x}Cu_xFe_2O_4$ ferrites prepared by sol−gel method and sintered at high temperature show the effect of copper doping on the structural and magnetic properties of nickel ferrites [9] due to formation of single phase spinel ferrite structure. Ferrospinels of nickel, cobalt and copper and their sulphated analogues prepared co-precipitation route were proved to be good catalysts for the benzoylation of

Corresponding author: H. NAYAK; E-mail: himansu110@gmail.com, drh_nayak@yahoo.com
DOI: 10.1016/S1003-6326(16)64135-3

toluene [10].

Copper−zinc ferrites crystallize in cubic spinel structure. The properties of Cu−Zn ferrites nanoparticle can be influenced by several factors, such as chemical composition, electronic configuration, ionic radius and synthesis techniques. Copper ferrite ($CuFe_2O_4$) is an interesting material and has been widely used for various applications, such as catalysts. Magnetic and electrical properties of Cu ferrites vary greatly with the change of chemical component and cation distribution. For instance, most of bulk $CuFe_2O_4$ has an inverse spinel structure, with 85% Cu^{2+} occupying site B whereas $ZnFe_2O_4$ is usually assumed to be a completely normal spinel and Zn^{2+} ions preferentially occupy site A while Fe^{3+} ions would be displaced from site A for site B. Zn-substitution results in a change of cations in chemical composition and a different distribution of cations between sites A and B. Consequently, the magnetic and electrical properties of spinel ferrites will change with changing cation [11]. Various investigations studied the electrical and thermal power of the spinel ferrites and found that they have semi-conducting properties of n- or p-type [12]. With a view to understand the conduction mechanism in mixed Cu−Zn ferrites, the semi-conducting properties as a function of composition and temperature, the results for such a study towards lanthanum oxalate decomposition are presented in this work.

The aim of this work is to present a novel and economical method for preparing Cu−Zn ferrite by the citrate precursor method in order to achieve lower sintering temperatures. The present work also highlights the preparation of zinc ferrite nanopowders and replacing zinc sites by copper using self combustion method following by thermal treatment and study the catalytic activity on lanthanum oxalate decomposition to CO and CO_2. The changes in the phase composition of materials after the catalytic test were also the investigation focus. The relationship among parameter of synthesis, phase composition, particle size, micro strain and catalytic behaviour of ferrite materials has been discussed.

2 Experimental

Preparation of lanthanum oxalate oxalates of La(III) was prepared as per our early work [13] using high purity AR grade $La(NO_3)_3$ and ammonium oxalate solution and finally dried at 80 ℃ to a constant mass. Four samples with chemical compositions as $ZnFe_2O_4$, $Zn_{0.75}Cu_{0.25}Fe_2O_4$, $Zn_{0.50}Cu_{0.50}Fe_2O_4$, and $Zn_{0.25}Cu_{0.75}$-Fe_2O_4 were prepared using following analytically pure (AR) grade $Zn(NO_3)_2{\cdot}6H_2O$ (287.49 g/mol), $Cu(NO_3)_2{\cdot}3H_2O$ (241.60 g/mol), and $Fe(NO_3)_3{\cdot}9H_2O$ (404 g/mol) as starting materials. Citric acid (AR grade, molecular mass: 210.14 g/mol) was used as chelating agent. The gel was subjected to calcination at 650 ℃ for 4.5 h in a furnace to obtain the combusted flake form material. By grinding the flakes in mortar and pestle, powdered form of material was obtained. The prepared samples have been referred to as F1, F2, F3, and F4, respectively.

Mixture of lanthanum oxalate was prepared with F1, F2, F3, and F4, in three different mole fractions, i.e. 2%, 5%, and 10% by grinding in an agate mortar. The mixture of uniform mesh size was subjected to thermogravimetric study using SCHIMADZU DTG 50 thermo analyser at a heating rate of 5 ℃/min.

3 Result and discussion

3.1 X-ray diffraction analysis

The observed XRD patterns of nano catalyst samples are shown in Fig. 1 and found to be in good agreement with the JCPDS card 82−1042 (Table 1). The XRD pattern shows single peak corresponding to each diffraction angle; hence, it shows the single phase of inverse spinel zinc copper ferrite. It is observed that the crystallite size of the composite ferrites increases with increasing the Cu content. This is due to the decrement in the densities of nucleation centres in the doped samples, which results in the formation of larger crystallite size. The average crystallite size was determined from the diffraction peak broadening with the use of the Scherrer equation.

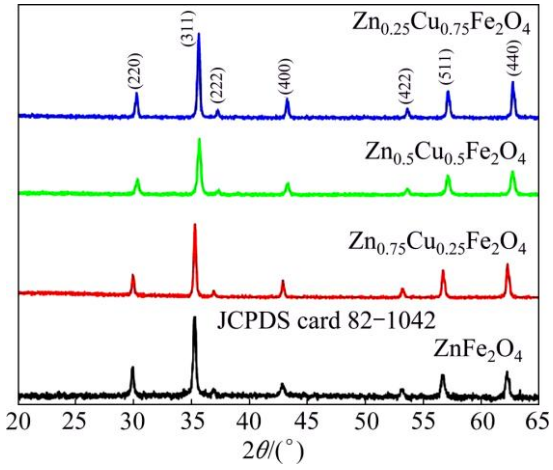

Fig. 1 XRD patterns for various types of prepared Zn−Cu ferrites

3.2 SEM analysis

Figure 2 shows the SEM images for all the prepared nano catalyst samples of ferrites. The SEM images show formation of the micro agglomerated particles and also some voids. Porosity is located at the junction of the agglomerates. It is clearly seen in the micrographs that

Table 1 XRD spectra of Zn−Cu ferrite nanoparticles

Zn−Cu ferrite	2θ/(°)	*d* spacing (observed)/Å	*d* spacing (JCPDS)/Å
$ZnFe_2O_4$	29.913	2.986	2.9851
	33.158	2.5517	2.5457
	36.877	2.4366	2.4347
	42.841	2.1102	2.1108
	53.142	1.7229	1.7234
	56.664	1.6239	1.6248
	62.21	1.4918	1.4925
$Zn_{0.75}Cu_{0.25}Fe_2O_4$	29.9547	2.9821	2.9851
	35.3146	2.5408	2.5457
	36.9433	2.4324	2.4347
	42.8465	2.1100	2.1108
	53.21	1.7209	1.7234
	56.6971	1.6230	1.6248
	62.2277	1.4914	1.4925
$Zn_{0.5}Cu_{0.5}Fe_2O_4$	30.3572	2.9435	2.9851
	35.6702	2.5163	2.5457
	37.393	2.4042	2.4347
	43.3111	2.0884	2.1108
	53.7481	1.7049	1.7234
	57.102	1.6125	1.6248
	62.6886	1.4813	1.4925
$Zn_{0.25}Cu_{0.75}Fe_2O_4$	30.1933	2.9591	2.9851
	35.5827	2.5223	2.5457
	37.2095	2.4156	2.4347
	43.1625	2.0952	2.1108
	53.5478	1.7108	1.7234
	57.0276	1.6144	1.6248
	62.6281	1.4828	1.4925

the grains of the Zn−Cu ferrite are very rough, which allow adsorption of oxygen species on the sensing surface. The results of the XRD and SEM divulge that all the samples are well crystalline nano sized spinel ferrites. The average particle diameter was found to be 29 nm, which agrees well with that estimated from XRD data.

3.3 FT-IR analysis

FT-IR spectra of the synthesized ferrite nanoparticles measured in the frequency range of 400−4000 cm^{-1} are shown in Fig. 3. Two prominent absorption bands around 400 and 600 cm^{-1}, respectively, are observed. These spectra represent characteristic features of ferrospinels, and bands are attributed to the stretching vibration due to the interaction between the oxygen atom and the cations in tetrahedral and octahedral sites, respectively. The difference between them is due to the

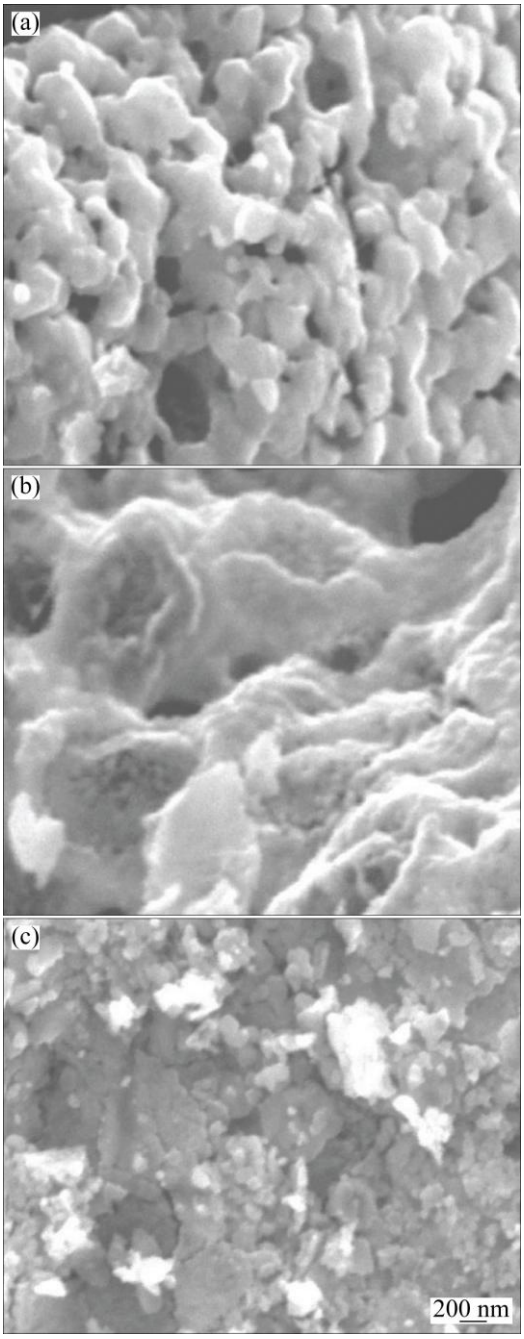

Fig. 2 SEM images of $Zn_{1.0}Cu_{0.0}Fe_2O_4$ (a), $Zn_{0.75}Cu_{0.25}Fe_2O_4$ (b) and $Zn_{0.25}Cu_{0.75}Fe_2O_4$ (c)

change in bond length (Fe—O) at the octahedral and tetrahedral sites. This difference in the band position is expected because of the difference in the Mn^{n+}—O^{2-} distance for the octahedral and tetrahedral compounds. In the vibrational spectra of ferrites, the sharp absorption band around 600 cm^{-1} is attributed to the intrinsic vibrations of the tetrahedral groups and the other band of the octahedral groups. There are two weak and broad absorptions around 1400 and 1600 cm^{-1} corresponding to the presence of small amount of residual carbon in the samples. These absorptions in the present case are very weak, which indicates that the residual carbon has mostly

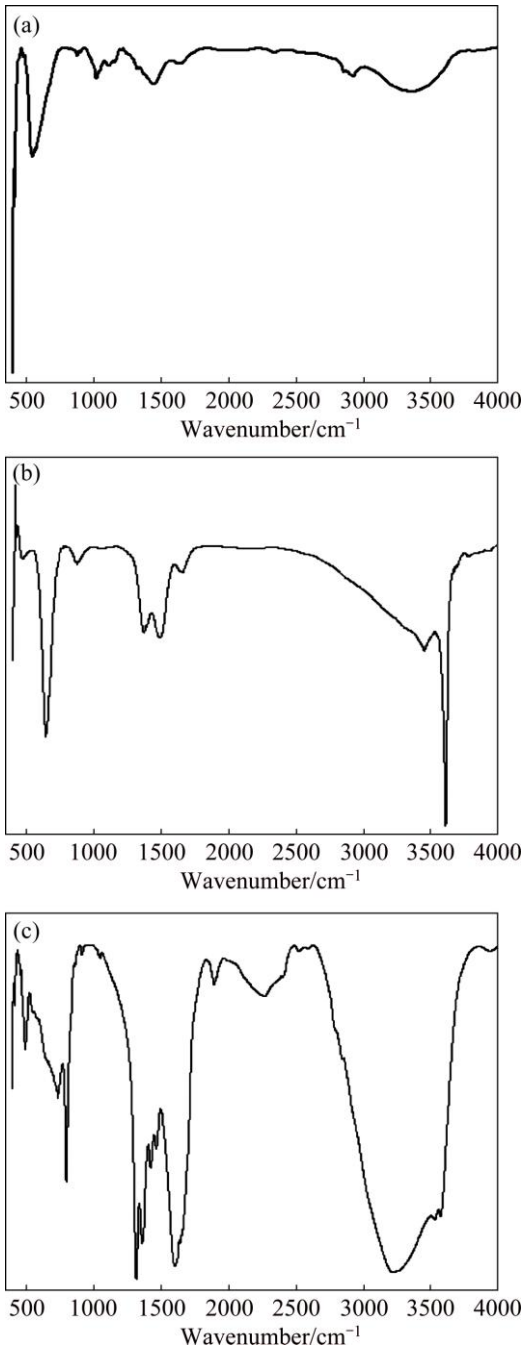

Fig. 3 FT-IR spectra of $Zn_{0.75}Cu_{0.25}Fe_2O_4$ (a), $La_2(C_2O_4)_3$ + $Zn_{0.75}Cu_{0.25}Fe_2O_4$ (b) and $La_2(C_2O_4)_3$ + $Zn_{0.75}Cu_{0.25}Fe_2O_4$ (5%) (c)

burnt away during the self-combustion process. The wave number of these absorptions indicates that this carbon is in the form of complex carbonates. Three distinct peaks are obtained at 1618 cm^{-1} (—C═O), 1316 cm^{-1} (C—O) and 795 cm^{-1} (La—O), suggesting the presence of the oxalate ion. The FI-IR spectrum of the products after TG at 490 ℃ suggests incomplete decomposition as evident from peaks obtained at 1432, 1100, 1000 and 858 cm^{-1}. A small peak at 1100 cm^{-1} concurrent with diminution of oxalate peak suggests a carbonate-like decomposition intermediate. A prominent peak at 1432 cm^{-1} is due to the carbonate ion.

3.4 Thermal analysis

Thermogravimetric curves for lanthanum oxalate and its mixture with samples F1, F2, F3 and F4 show significant increase in extent of conversion α with respect to pure lanthanum oxalate although the decomposition temperature remains undisturbed, i.e., at 653 K (Fig. 4). Mixture of lanthanum oxalate with F1 has low fractional decomposition α at the start of the decomposition compared with that of lanthanum oxalate, but after attaining the temperature 683 K, the α value increases significantly till the completion of the reaction (Fig. 4).

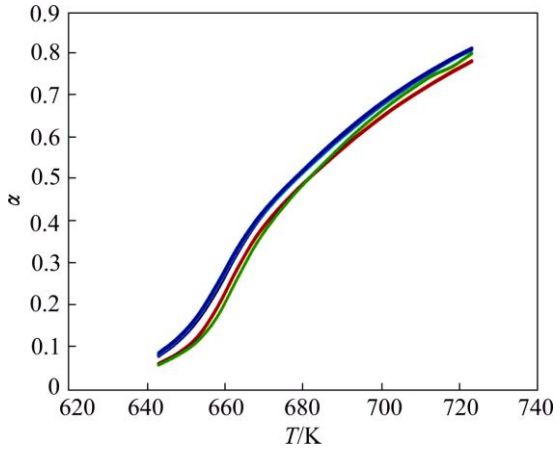

Fig. 4 α–T curves for decomposition of pure lanthanum oxalate (red), lanthanum oxalate mixed with $ZnFe_2O_4$ (5%) (red), $Zn_{0.75}Cu_{0.25}Fe_2O_4$ (5%) (blue), $Zn_{0.5}Cu_{0.5}Fe_2O_4$ (2%) (green), and $Zn_{0.25}Cu_{0.75}Fe_2O_4$(10%) (violet)

However, the incorporation of Cu in the Zn lattice and the mixture of lanthanum oxalate with F2, F3 and F4 make the decomposition process facile at low decomposition temperature, i.e., 648 K. It is found that $Zn_{0.75}Cu_{0.25}Fe_2O_4$ is the ideal composition showing the highest value for α although the decomposition curves are indistinguishable in the graph. Under high resolution (Fig. 5), the trend follows the order of F2>F4>F3.

The derivative curves are also shown in Fig. 6, signifying the temperature corresponding to the highest rate of decomposition α_{max} to be 659 K. Samples prepared with three different mole fractions of spinel ferrites F2 show trends with no remarkable change in fractional decomposition α. But at low content of catalyst (2%, mole fraction), α value is the highest as the temperature gradually increases up to 663 K, contents of 5% and 10% show equal activities but after that 10% gets higher value of fractional decomposition α till the completion of reaction (Fig. 6).

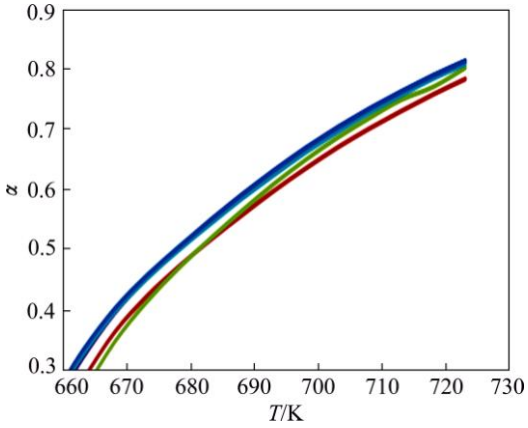

Fig. 5 Enlarged $\alpha-T$ curves for decomposition of pure lanthanum oxalate(red), lanthanum oxalate mixed with $ZnFe_2O_4$ (5%) (red), $Zn_{0.75}Cu_{0.25}Fe_2O_4$(5%) (blue), $Zn_{0.5}Cu_{0.5}$-Fe_2O_4 (2%) (green), $Zn_{0.25}Cu_{0.75}Fe_2O_4$(10%) (violet)

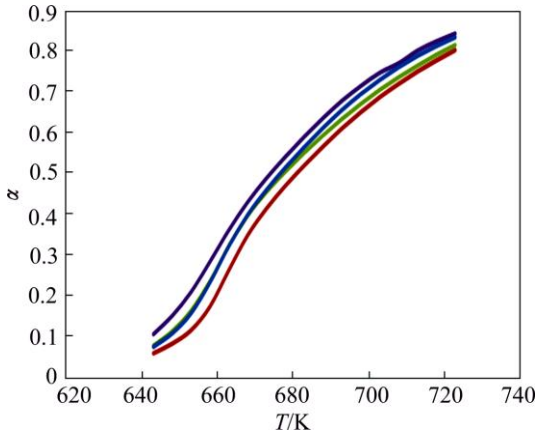

Fig. 6 $\alpha-T$ curves for decomposition of lanthanum oxalate mixed with $ZnFe_2O_4$(5%) (red), $Zn_{0.75}Cu_{0.25}Fe_2O_4$(5%) (green), $Zn_{0.75}Cu_{0.25}Fe_2O_4$(2%) (violet), $Zn_{0.75}Cu_{0.25}Fe_2O_4$(10%) (blue)

3.5 Kinetic analysis

The catalytic activity of mixed metal spinel ferrites of Cu−Zn at the same temperature was found to be greater than that of Zn ferrite. The completion of reaction takes place in one step in the case of pure lanthanum oxalate and so also its mixture with mixed metal spinel ferrites of the Cu−Zn. For comparative study, all the data are analyzed for the one step process. The kinetic parameters for the decomposition stage were determined using the Coat−Redfern equation:

$$\lg g(\alpha)/T^2=\lg(AR/\beta E)-E/(2.0303RT) \quad (1)$$

where A is the pre-exponential factor, β is the heating rate, E is the activation energy, R is the mole gas constant and T is the thermodynamic temperature. $\lg g(\alpha)/T^2$ is calculated for each possible rate controlling mechanism using various solid state models and plotted against $1/T$ (Figs. 7 and 8), using the best fit model for the reaction.

The value of $g(\alpha)$ with the highest coefficient of

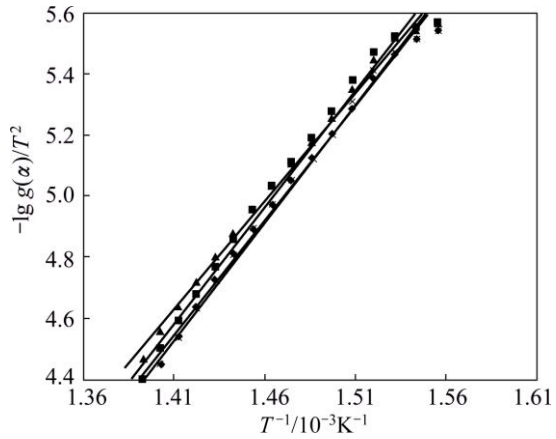

Fig. 7 Variation of $-\lg g(\alpha)/T^2$ against $1/T$ using F3 mechanism for $La_2(C_2O_4)_3$ + $ZnFe_2O_4$ (5%) (red), $La_2(C_2O_4)_3$ (green), $La_2(C_2O_4)_3$ + $Zn_{0.75}Cu_{0.25}Fe_2O_4$ (5%) (blue), $La_2(C_2O_4)_3$+ $Zn_{0.5}Cu_{0.5}Fe_2O_4$ (5%) (star), $La_2(C_2O_4)_3$+$Zn_{0.25}Cu_{0.75}$ Fe_2O_4(5%) (star)

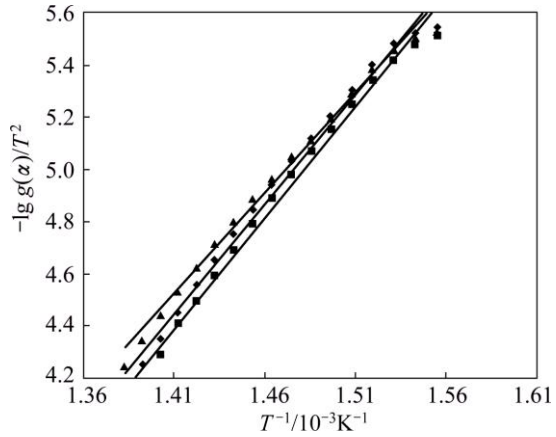

Fig. 8 Variation of $-\lg g(\alpha)/T^2$ against $1/T$ using F3 mechanism for $Zn_{0.75}Cu_{0.25}Fe_2O_4$(2%) (red), $Zn_{0.75}Cu_{0.25}$ Fe_2O_4(5%) (green), $Zn_{0.75}Cu_{0.25}Fe_2O_4$(10%) (blue)

linear regression analysis, r gives the idea about the best fit model function. The best fit model F_3, i.e., the third order law is chosen for the entire temperature range 643−723 K in order to compare all the data. The activation energy, E and pre-exponential factor A were calculated from the slope and intercept respectively of the Coat−Redfern equation and the plausible mechanism and the corresponding kinetic and thermodynamic parameters are listed in Tables 2 and 3 using the following equations:

$$\Delta H^*=E-RT \quad (2)$$

$$\Delta S^*=R\{\ln\ [hA/(k_BT)]-1\} \quad (3)$$

$$\Delta G^*=\Delta H^*-T\Delta S^* \quad (4)$$

where ΔH^*, ΔS^* and ΔG^* are the enthalpy, entropy and free energy changes of activation, respectively; h is the Plank's constant and k_B is the Boltzman's constant.

The rate of the reaction was determined corresponding to the highest value of fraction decomposed, α_{max}, which is the peak of the curves, corresponding to temperature T (403 ℃ or 675 K) in the DTG plots (Fig. 9).

The rate constant k has got the highest value for F4 almost same as that of F2 with 5% content and the highest value may be attributed to high copper content. The higher catalytic activity may be due to the fact that beside the one component sites Cu^{2+}−Cu^{+}, Fe^{3+}−Fe^{2+}, there will be also the mixed sites Cu^{2+}−Fe^{+} and/or Cu^{+}−Fe^{2+} ion pairs as a result of mutual charge interaction. In other words, the increasing activity of mixed oxides might be attributed to increase in the content of active sites via creation of new ion pairs.

$$C_2O_4^{2-} \rightarrow C_2O_4^{-} + e \quad (5)$$

$$Cu^{2+} + e \rightarrow Cu^{+} \quad (6)$$

$$Fe^{3+} + e \rightarrow Fe^{2+} \quad (7)$$

$$Cu^{+} + Fe^{3+} \rightarrow Cu^{2+} + Fe^{2+} \quad (8)$$

Table 2 Arrhenius parameters for decomposition of various samples using Coat−Redfern equation

Sample	E(±0.05)/(kJ mol^{-1})	lg[A(±0.02)/s^{-1}]	k*(±0.05)/s^{-1}	ΔH*/(kJ mol^{-1} K^{-1})	ΔS*/(J mol^{-1})	ΔG*/(kJ mol^{-1})
Pure $La_2(C_2O_4)_3$	135.523	10.26	0.3307	−130.044	−63.41	−87.242
$La_2(C_2O_4)_3$+F1	146.609	11.16	0.3474	−141.131	−46.18	−109.959
$La_2(C_2O_4)_3$+F2	147.681	11.29	0.3854	−142.202	−43.69	−112.711
$La_2(C_2O_4)_3$+F3	144.024	10.96	0.3512	−138.545	−50.61	−104.383
$La_2(C_2O_4)_3$+F4	145.384	11.11	0.3872	−139.905	−47.14	−108.085

Table 3 Arrhenius parameters for decomposition of various samples using Coat−Redfern equation

Sample	E(±0.05)/(kJ mol^{-1})	lg[A(±0.02)/s^{-1}]	k*(±0.05)/s^{-1}	ΔH*/(J mol^{-1} K^{-1})	ΔS*/(J mol^{-1})	ΔG*/(kJ mol^{-1})
$La_2(C_2O_4)_3$+F4(2%)	163.650	12.65	0.479	−158.171	−17.56	−146.318
$La_2(C_2O_4)_3$+F4(5%)	145.384	11.11	0.3872	−139.905	−47.14	−108.085
$La_2(C_2O_4)_3$+F4(10%)	161.678	12.45	0.4331	−156.199	−21.48	−141.700

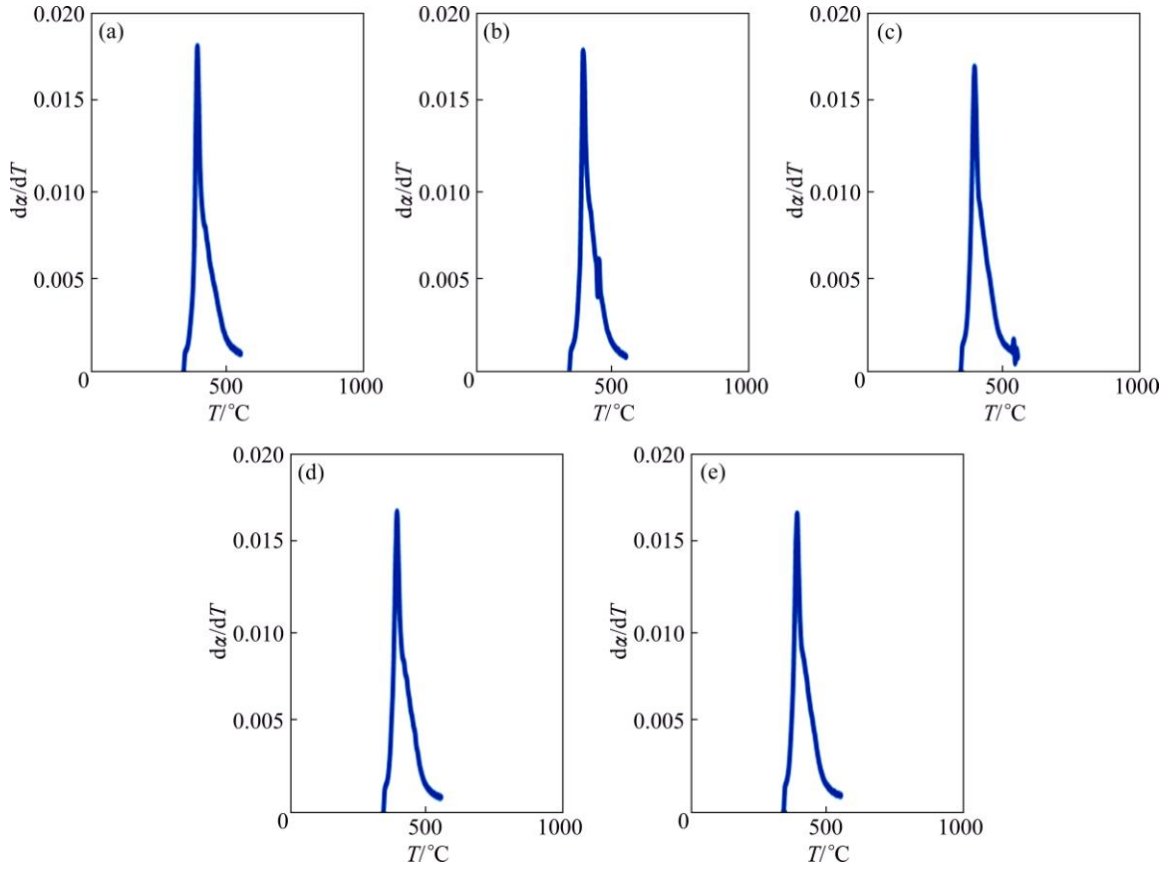

Fig. 9 DTG plots of different samples: (a) Lanthanum oxalate; (b) Lanthanum oxalate + $ZnFe_2O_4$; (c) Lanthanum oxalate + $Cu_{0.25}Zn_{0.75}Fe_2O_4$; (d) Lanthanum oxalate + $Cu_{0.5}Zn_{0.5}Fe_2O_4$; (e) Lanthanum oxalate + $Cu_{0.75}Zn_{0.25}Fe_2O_4$

4 Role played by spinel ferrites

In $Zn_xFe_{3-x}O_4$, the Zn-substituted magnetite could be presented with the formulas $(Zn^{2+}{}_xFe^{3+}{}_{1-x})_{tetra}$-$[Fe^{3+}{}_{1+x}Fe^{2+}{}_{1+x}]_{octa}O_4$, as the spinel structure is preserved in the range $0\leq x\leq 1$. Samples having higher zinc content are weak tetrahedral A-site and octahedral B-site super exchange interaction. The conduction at lower temperature is due to hopping of electrons between Fe^{3+} and Fe^{2+} ions, whereas at higher temperature due to polaron hopping. In addition, the increase of Zn content is associated with a decrease in copper content. In turn, the possibility of Cu^+ formation and $Cu^{2+}\leftrightarrow Cu^+$ hopping process and the number of holes involved will be reduced. While heating $CuFe_2O_4$ sample, two temperature domains are noted in which the concentration of B-site Cu^{2+} ions is increased and the interstice cation exchange is given as

$$Cu^{2+}{}_A+Fe^{3+}{}_B\rightarrow Cu^{2+}{}_B+Fe^{3+}{}_A \quad (9)$$

This reaction gives n-type condition, while at low temperature, the conduction process for $CuFe_2O_4$ at lower temperature is

$$Cu^{+}{}_A+Cu^{2+}{}_A\rightarrow Cu^{2+}{}_A+Cu^{+}{}_A \quad (10)$$

This gives only p-type conduction depending on the relative concentration of Cu^+ or Cu^{2+} ions at site A. This gives only p-type conduction depending on the relative concentration of Cu^+ of Cu^{2+} ions at site A. While as the zinc content is increased, Cu content tends to decrease at site A. As Zn content x is explained on the basis of difference in the ionic radii of Cu^{2+} and Zn^{2+}, the $Cu_{1-x}Zn_xFe_2O_4$ system has a cubic spinel configuration with unit cell consisting of eight formula units of $(Zn_xFe_{1-x})_A[Cu_{1-x}Fe_{1+x}]_BO_4$. The Cu^{2+} ions have preference for the octahedral sites and Zn^{2+} ions have preference for the tetrahedral sites. The observed linear increase of lattice constant with Zn content x can be attributed to the large ionic radius of Zn^{2+} (0.84 Å) as compared to the ionic radius of Cu^{2+} (0.79 Å). The larger ionic radius of Zn^{2+} replaces the smaller ionic radius of Cu^{2+} variation of catalytic activity of ferrite powders which are probably due to the changes of the valence state of catalytically active components of the ferrite powders. The catalytic oxidation reactions of carbon monoxide released from lanthanum oxalate [11], by metal ferrite can be written in the following equations:

$$La_2(C_2O_4)_3\rightarrow La_2(CO_3)_3+3CO\rightarrow La_2O(CO_3)_2+CO_2 \quad (11)$$

$$La_2O(CO_3)_2\rightarrow La_2O(CO_3)+CO_2 \quad (12)$$

$$MFe_2O_4+xCO\rightarrow MFe_2O_{4-x}+xCO_2 \quad (13)$$

$$MFe_2O_{4-x}+0.5xO_2\rightarrow MFe_2O_4 \quad (14)$$

According to the contact catalysis theory, the surface reaction involves five consecutive steps: 1) Diffusion of CO and O_2 to the surface of the ferrite; 2) The gas molecules adsorb preferentially on the surface of the ferrite and due to chemisorption of gas molecules, the oxygen in the ferrite transfers from the bulk to the chemisorbed species; 3) CO_2 is produced by the reaction of CO and O_2 on the surface of the catalyst; 4) The produced CO_2 molecules are then released from the interface and leave sites for other CO and O_2 gas molecules adsorption; 5) Finally, the produced gas diffused into the main body of the gas.

5 Conclusions

1) The Cu−Zn ferrite behaves as n-type semiconductor.

2) The transition from tetragonal structure to cubic was found to decrease with increasing Zn content.

3) The conduction at lower temperature is due to hopping of electrons between Fe^{3+} and Fe^{2+} ions, whereas at higher temperature due to polaron hopping.

4) The XRD analysis reveals the formation of single phase spinel structure at very low annealing temperature without any secondary phases. The particle size was observed to decrease with increasing Zn content probably due to the reaction temperature and time.

5) The lattice parameters were observed to increase with increasing Zn content, which is due to large ionic radii of zinc when compared with copper ions.

6) The increase in zinc content increases particle size thereby providing comparatively less surface area for the catalytic activities, hence, $Zn_{0.25}Cu_{0.75}Fe_2O_4$ is the best suitable catalyst out of the four.

References

[1] SUGIMOTO M. The past, present, and future of ferrites [J]. Journal of the American Ceramic Society, 1999, 82: 269−280.

[2] SUZUKI Y. Epitaxial spinel ferrite thin films [J]. Annual Review of Material Research, 2001, 31: 265−289.

[3] NAYAK H, JENA A K. Catalyst effect of transition metal nano oxides on the decomposition of lanthanum oxalate hydrate: A thermogravimetric study [J]. International Journal of Science and Research, 2014, 3: 381−388.

[4] SINGH R K, YADAV A, PRASAD K, NARAYAN A. Dependence of magnetic and structural properties of $Ni_{0.5}M_{0.5}Fe_2O_4$ (M=Co, Cu) nanoparticles synthesized by citrate precursor method on annealing temperature [J]. International Journal of Engineering, Science and Technology, 2010, 2: 73−79.

[5] JOELDA D, SANTOSA J R D, CUNHAA R B L, KIMINAMIB R H G A, MELLO COSTAA A C F. Use of Ni−Zn ferrites doped with Cu as catalyst in the transesterification of soybean oil to methyl esters [J]. Materials Research, 2013, 16: 625−627.

[6] PRABHULKAR S G, PATIL R M. Synthesis, characterization and catalytic properties of nickel substituted copper ferrospinel nanoparticles [J]. Research Journal of Material Sciences, 2013, l: 18−21.

[7] NAYAK H. Kinetic and thermodynamic studies on the non-isothermal decomposition of lanthanum oxalate hydrate, catalysed by transition metal nano oxides [J]. IOSR Journal of Applied Chemistry, 2014, 7: 15−23.
[8] VINUTHNA C H, RAVINDER D, MADHUSUDAN R, RAVINDER D. Characterization of $Co_{1-x}Zn_xFe_2O_4$ nano spinal ferrites prepared by citrate precursor method [J]. Int Journal of Engineering Research and Applications, 2013, 3: 654−660.
[9] KUMAR G R, KUMAR K V, VENUDHAR Y C. Synthesis, structural and magnetic properties of copper substituted nickel ferrites by sol−gel method [J]. Materials Sciences and Applications, 2012, 3: 87−91.
[10] RAMANKUTTY C G, SUGUNAN S. Surface properties and catalytic activity of ferrospinels of nickel, cobalt and copper, prepared by soft chemical methods [J]. Applied Catalysis A: General, 2001, 218: 39−51.
[11] ANJANEYULU T, NARAYANA M P, NARENDRA K, VIJAYA K K. Structural and magnetic properties of $Cu_{1-x}Zn_xFe_2O_4$ nano-powders synthesized by oxalate based precursor method [J]. International Journal of Basic and Applied Chemical Sciences, 2013, 3: 50−59.
[12] DAWOUD A E. Thermoelectric power of Cu−Zn ferrites [J]. Materials Sciences and Applications, 2011, 2(11): 1572−1577.
[13] NAYAK H, PATI S K, BHATTA D. Decomposition of γ-irradiated $La_2(C_2O_4)_3 + CuO$ mixture: A non-isothermal study [J]. Radiation Effects and Defects in Solids, 2004, 159: 93−106.

锌−铜混合纳米铁氧体催化活性对草酸镧分解动力学的影响

H. NAYAK

Department of Chemistry, Orissa University of Agriculture and Technology, Bhubaneswar 751003(Orissa), India

摘　要：采用溶胶−凝胶法合成纳米结构锌−铜混合铁氧体。XRD 分析表明，不同组分 $Zn_{(1-x)}Cu_xFe_2O_4$ (x=0.0, 0.25, 0.50, 0.75)铁氧体为单相反尖晶石结构。随着铜含量的增加，晶粒尺寸增大。采用 SEM 表征样品的表面形貌，结果表明粒子为多孔结构。采用 FT-IR 和 TEM 分析所制备的样品。当 x=0.75 及催化剂为 5%(摩尔分数)时，速率常数 k 值最高，这归因于高铜含量以及除 Cu^{2+}−Cu^{+}和 Fe^{3+}−Fe^{2+}外，由于电荷相互作用而产生的混合位 Cu^{2+}−Fe^{+}和/或 Cu^{+}−Fe^{2+}离子对。混合氧化物活性增加归因于通过新离子产生而增大的活性位置浓度。随着锌含量的增加，颗粒尺寸增大。铁氧体粉末催化活性的变化是因为催化活性组分价态的变化，这能氧化从草酸镧中释放的一氧化碳。

关键词：混合铁氧体；尖晶石；价态感应；催化活性；速率常数；草酸镧

(Edited by Xiang-qun LI)